

# Computer Methods in Biomechanics and Biomedical Engineering

ISSN: 1025-5842 (Print) 1476-8259 (Online) Journal homepage: [www.tandfonline.com/journals/gcmb20](http://www.tandfonline.com/journals/gcmb20)

## Numerical simulation of a normalized time-fractional SUC epidemic model

Chaeyoung Lee , Jyoti , Soobin Kwak , Yunjae Nam , Hyundong Kim & Junseok Kim

**To cite this article:** Chaeyoung Lee , Jyoti , Soobin Kwak , Yunjae Nam , Hyundong Kim & Junseok Kim (16 Sep 2025): Numerical simulation of a normalized time-fractional SUC epidemic model, Computer Methods in Biomechanics and Biomedical Engineering, DOI: [10.1080/10255842.2025.2556313](https://doi.org/10.1080/10255842.2025.2556313)

**To link to this article:** <https://doi.org/10.1080/10255842.2025.2556313>



Published online: 16 Sep 2025.



Submit your article to this journal



Article views: 31



View related articles



CrossMark

View Crossmark data



## Numerical simulation of a normalized time-fractional SUC epidemic model

Chaeyoung Lee<sup>a</sup>, Jyoti<sup>b</sup>, Soobin Kwak<sup>c</sup>, Yunjae Nam<sup>d</sup>, Hyundong Kim<sup>e</sup> and Junseok Kim<sup>c</sup>

<sup>a</sup>Department of Mathematics, Kyonggi University, Suwon, Republic of Korea; <sup>b</sup>The Institute of Basic Science, Korea University, Seoul, Republic of Korea; <sup>c</sup>Department of Mathematics, Korea University, Seoul, Republic of Korea; <sup>d</sup>Program in Actuarial Science and Financial Engineering, Korea University, Seoul, Republic of Korea; <sup>e</sup>Department of Mathematics and Physics, Gangneung-Wonju National University, Gangneung, Republic of Korea

### ABSTRACT

We develop a normalized time-fractional susceptible-unidentified infected-confirmed (SUC) epidemic model that incorporates memory effects through fractional calculus to capture non-local time interactions. Unlike integer-order models, this model reflects how past states influence present transmission. Numerical simulations show that smaller fractional orders accelerate the decline of susceptible individuals and produce faster but lower infection peaks, while larger orders yield slower, oscillatory declines and delayed peaks, indicating prolonged outbreaks. Moreover, the confirmation parameter critically shapes epidemic dynamics, as higher values reduce infection spread and lower peak levels of unidentified and confirmed cases, and this result highlights its role in controlling epidemic progression.

### ARTICLE HISTORY

Received 8 May 2025

Accepted 25 August 2025

### KEYWORDS

Computer simulation; finite difference scheme; normalized time-fractional SUC equation

## 1. Introduction

The novel coronavirus, first detected in 2019 and named COVID-19, rapidly spread from China to countries across the globe. Despite various government-imposed measures to curb its transmission (Ayouni et al. 2021; Lv et al. 2022; Li and Zhang 2023; Williams et al. 2023), the spread of COVID-19 continued, and various variants were identified over time (Liu et al. 2020). It is essential to understand that viral mutations build on previous strains through accumulated genetic changes (Korber et al. 2020; Xu et al. 2022). This highlights the necessity of incorporating non-integer order fractional derivatives in modeling the dynamics of COVID-19 (Baba and Rihan 2022; Fatima et al. 2024; Shahabifar et al. 2024; Thirumalai et al. 2025). In recent years, various mathematical models have been developed to focus on epidemic diseases (Alsaadi et al. 2023; Hwang et al. 2024). For example, Salman et al. (2021) presented an SIRS model that identified how the trajectories of COVID-19 infection spread over time by fitting the model to real COVID-19 data released by the Ministry of Health Malaysia. Besalú and Binotto (2023) extended a stochastic SIR-type epidemic model by incorporating time-dependent daily encounters and a quarantine parameter, and provided an analytic description and examined its dynamics through

diffusion approximations, simulations, and real disease applications. Çar and Çelik (2022) studied the numerical solution of the SIR model for COVID-19's spread in Turkey using the Taylor matrix and collocation method, and analyzed transmission and recovery rates with data from March 2020 to July 2021 to predict the pandemic's evolution and provide graphical estimates. Zhao and Shi (2023) analyzed a stochastic SIR model with nonlinear incidence and recovery rates, and proved the existence of a global positive solution, established conditions for disease extinction or persistence, and demonstrated a stationary distribution under certain parameters, with theoretical results confirmed through numerical simulations. Sene (2020) extended a delayed SIR epidemic model using a fractional derivative with a Mittag–Leffler kernel. Alharthi and Jeelani (2023) investigated an SEIR model for COVID-19 using fractional calculus, performed qualitative analysis through the fixed point approach and computational analysis via simulations with fractional order derivatives, and compared real data with numerical results obtained using a scheme based on Newton's polynomials. Witbooi et al. (2023) presented a compartmental model for COVID-19, which incorporates vaccination and infected inflow, analyzed equilibrium stability, and performed numerical simulations based on South African data to

support the theoretical findings. Fan and Li (2023) presented a model that analyzed the impact of periodic environmental changes on the transmission of infectious diseases, particularly respiratory and enteric diseases. They used periodic functions for pathogen transmission and decay rates to reflect the influence of environmental fluctuations and verified that the model incorporating periodic factors provided more accurate predictions of seasonal disease patterns, such as COVID-19, compared to non-periodic models.

Zhang et al. (2020) proposed the application of time-fractional derivative equations for modeling COVID-19 dynamics and relief scenarios. They verified that while general transmission and recovery align with integral-order models, the evolution of the death toll is effectively captured by time fractional-derivative equations due to inherent time memory effects. Majee et al. (2022) presented and analyzed a new fractional-order SIR type epidemic model that includes a saturated treatment function in order to provide more profound insights into disease systems. The authors emphasized that fractional-order systems are crucial for an accurate representation of the memory effect in disease transmission. This property allows susceptible populations to rely on past experiences as a means of infection prevention. They also noted the practical advantage of such systems as the initial conditions can be directly interpreted, similar to those of integer-order differential equations. Bouissa et al. (2023) investigated a diffusive SIR epidemic model, characterized by reaction-diffusion equations augmented with a Caputo fractional derivative. This formulation includes a critical memory effect to better reflect disease history. It emphasizes that the non-locality of these fractional operators allows for a thorough consideration of the disease's entire evolution history, which can reduce errors when fitting real data.

More recently, Kim (2024) proposed a new normalized time-fractional SIR model that includes memory effects. Al-Zahrani et al. (2022) investigated the effects of the contact rate between people through a susceptible-infected-treatment-recovered (SITR) fractional derivative equation. Also, Yousif et al. (2023) implemented a fractional-order SEIRD model for studying the COVID-19 epidemic and stated that due to the value of the reproduction number, which is greater than one, the disease outbreak would continue for several more months and require additional control measures.

The novelty of the paper is the proposal of a normalized time-fractional epidemic model, which emphasizes a normalized formulation and specialized compartments to effectively incorporate memory effects. This model provides a more realistic and

accurate description of epidemics like COVID-19. As future work, we intend to investigate the inverse problem of estimating the unidentified confirmed infection population in time-fractional epidemic models (Shaikh et al. 2020; Zhang et al. 2020; Santra et al. 2024; Ur Rahman et al. 2025), through the application of the least-squares curve fitting method to real data (Hwang et al. 2024).

This paper is organized as follows. Section 2 presents the proposed normalized time-fractional SUC epidemic model. Section 3 presents the computational solution algorithm. Section 4 provides computational experiments to highlight the effect of the fractional order on the temporal evolution of each population. Finally, Section 5 provides the conclusion of the paper.

## 2. Proposed normalized time-fractional SUC epidemic model

Unlike typical epidemic diseases, COVID-19 presents unique characteristics, where infected individuals are generally isolated, reducing transmission to others except in rare cases. Consequently, a novel model specialized for the COVID-19 pandemic was required, and a susceptible-unidentified infected-confirmed (SUC) model was introduced, which shares an equivalent framework to the SIR model but with distinct meanings for each compartment. Confirmed populations are individuals who have undergone diagnostic testing and have been officially confirmed as infected cases. These individuals are recognized as known cases within the public health system. Once confirmed, they are typically subjected to isolation or quarantine measures to prevent further transmission of the disease. This compartment reflects the group of patients who are not only identified but also actively managed through medical supervision and public health interventions. For more information, see (Chen et al. 2024) and references therein. In this paper, we incorporate the memory effect into the SUC model by proposing a normalized time-fractional SUC model. This model is derived from the normalized time-fractional diffusion equation and the SIR model (Jornet and Nieto 2024; Kim 2024; Lee et al. 2024).

$$\frac{d^\alpha S(t)}{dt^\alpha} = \mu N - \beta \frac{S(t)U(t)}{N} - \mu S(t), \quad (1)$$

$$\frac{d^\alpha U(t)}{dt^\alpha} = \beta \frac{S(t)U(t)}{N} - \gamma U(t) - \mu U(t), \quad (2)$$

$$\frac{d^\alpha C(t)}{dt^\alpha} = \gamma U(t) - \mu C(t), \quad (3)$$

where  $S(t)$ ,  $U(t)$ , and  $C(t)$  are the susceptible, unidentified infected, and confirmed populations at time  $t$ ,

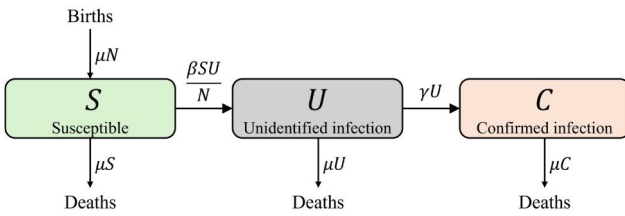


**Figure 1.** Schematic illustration of SUC model.

respectively. The parameter  $\beta$  is the rate at which the disease spreads among individuals,  $\gamma$  is the reciprocal of the number of days until confirmation of the diagnosis, and  $\mu$  is the birth and death rate (see Figure 1). The total population  $N = S(t) + U(t) + C(t)$  is assumed to be constant, as the birth rate equals the death rate.

$$\frac{d^\alpha S(t)}{dt^\alpha} = \frac{1-\alpha}{t^{1-\alpha}} \int_0^t \frac{dS(s)}{ds} \frac{ds}{(t-s)^\alpha}, \quad 0 < \alpha < 1. \quad (4)$$

Equation (4) is a normalized derivative, i.e.

$$\frac{1-\alpha}{t^{1-\alpha}} \int_0^t \frac{ds}{(t-s)^\alpha} = 1, \quad 0 < \alpha < 1. \quad (5)$$

Similarly,  $d^\alpha U(t)/dt^\alpha$  and  $d^\alpha C(t)/dt^\alpha$  are analogously defined. We note that the specific form of the normalized time-fractional derivative Equation (4) was obtained by modifying the original Caputo derivative by changing the constant coefficient of the integral using a time-dependent term that satisfies Equation (5), irrespective of time and the fractional orders. Please refer to Kim (2024) and the references therein for more detailed information.

### 3. Computational solution algorithm

We define  $S_n = S(t_n)$ ,  $U_n = U(t_n)$ , and  $C_n = C(t_n)$  for  $n = 1, \dots$ , where  $t_n = (n-1)\Delta t$ . We discretize Equation (4) in the following manner:

$$\begin{aligned} \frac{d^\alpha S(t_{n+1})}{dt^\alpha} &= \frac{1-\alpha}{t_{n+1}^{1-\alpha}} \sum_{p=1}^n \int_{t_p}^{t_{p+1}} \frac{dS(s)}{ds} \frac{ds}{(t_{n+1}-s)^\alpha} \\ &\approx \sum_{p=1}^n \frac{1-\alpha}{t_{n+1}^{1-\alpha}} \int_{t_p}^{t_{p+1}} \frac{ds}{(t_{n+1}-s)^\alpha} \frac{S_{p+1} - S_p}{\Delta t} \\ &= \sum_{p=1}^n \frac{(n+1-p)^{1-\alpha} - (n-p)^{1-\alpha}}{n^{1-\alpha}} \frac{S_{p+1} - S_p}{\Delta t}. \end{aligned} \quad (6)$$

Therefore, we derive

$$\sum_{p=1}^n w_p^n \frac{S_{p+1} - S_p}{\Delta t} = \mu N - \beta \frac{S_{n+1} U_n}{N} - \mu S_{n+1}, \quad (7)$$

$$\sum_{p=1}^n w_p^n \frac{U_{p+1} - U_p}{\Delta t} = \beta \frac{S_{n+1} U_n}{N} - \gamma U_{n+1} - \mu U_{n+1}, \quad (8)$$

$$\sum_{p=1}^n w_p^n \frac{C_{p+1} - C_p}{\Delta t} = \gamma U_{n+1} - \mu C_{n+1}. \quad (9)$$

Here,  $w_p^n = [(n+1-p)^{1-\alpha} - (n-p)^{1-\alpha}]/n^{1-\alpha}$ , which results in  $\sum_{p=1}^n w_p^n = 1$ . Equations (7)–(9) can be rewritten as follows:

$$\begin{aligned} w_n^n \frac{S_{n+1} - S_n}{\Delta t} &= \mu N - \beta \frac{S_{n+1} U_n}{N} - \mu S_{n+1} \\ &\quad - \sum_{p=1}^{n-1} w_p^n \frac{S_{p+1} - S_p}{\Delta t}, \end{aligned} \quad (10)$$

$$\begin{aligned} w_n^n \frac{U_{n+1} - U_n}{\Delta t} &= \beta \frac{S_{n+1} U_n}{N} - \gamma U_{n+1} - \mu U_{n+1} \\ &\quad - \sum_{p=1}^{n-1} w_p^n \frac{U_{p+1} - U_p}{\Delta t}, \end{aligned} \quad (11)$$

$$w_n^n \frac{C_{n+1} - C_n}{\Delta t} = \gamma U_{n+1} - \mu C_{n+1} - \sum_{p=1}^{n-1} w_p^n \frac{C_{p+1} - C_p}{\Delta t}, \quad (12)$$

Equations (10)–(12) are rewritten as

$$\begin{aligned} S_{n+1} &= \left( \frac{w_n^n S_n}{\Delta t} + \mu N - \sum_{p=1}^{n-1} w_p^n \frac{S_{p+1} - S_p}{\Delta t} \right) \\ &\quad / \left( \frac{w_n^n}{\Delta t} + \frac{\beta U_n}{N} + \mu \right), \end{aligned} \quad (13)$$

$$\begin{aligned} U_{n+1} &= \left( \frac{w_n^n U_n}{\Delta t} + \beta \frac{S_{n+1} U_n}{N} - \sum_{p=1}^{n-1} w_p^n \frac{U_{p+1} - U_p}{\Delta t} \right) \\ &\quad / \left( \frac{w_n^n}{\Delta t} + \gamma + \mu \right), \end{aligned} \quad (14)$$

$$\begin{aligned} C_{n+1} &= \left( \frac{w_n^n C_n}{\Delta t} + \gamma U_{n+1} - \sum_{p=1}^{n-1} w_p^n \frac{C_{p+1} - C_p}{\Delta t} \right) \\ &\quad / \left( \frac{w_n^n}{\Delta t} + \mu \right). \end{aligned} \quad (15)$$

We may use a high-order computational algorithm such as the Runge–Kutta method (Yang et al. 2024), which improves the accuracy of the approximation and is particularly useful for handling fractional-order systems over long time intervals where low-order methods may accumulate noticeable errors.

#### 4. Computational experiments

Computational results are obtained by solving Equations (13)–(15) with given initial conditions and parameter values. All calculations are conducted with a discrete temporal step size of  $\Delta t = 0.01$ . Let us consider a steady state as  $t$  approaches infinity:

$$\frac{d^\alpha S(t)}{dt^\alpha} = \frac{d^\alpha U(t)}{dt^\alpha} = \frac{d^\alpha C(t)}{dt^\alpha} = 0, \quad (16)$$

then Equations (1)–(3) become

$$\mu N - \beta \frac{S^* U^*}{N} - \mu S^* = 0, \quad (17)$$

$$\beta \frac{S^* U^*}{N} - \gamma U^* - \mu U^* = 0, \quad (18)$$

$$\gamma U^* - \mu C^* = 0, \quad (19)$$

where  $S^* = \lim_{t \rightarrow \infty} S(t)$ ,  $U^* = \lim_{t \rightarrow \infty} U(t)$ , and  $C^* = \lim_{t \rightarrow \infty} C(t)$ . Solving Equations (17)–(19) results in the equilibrium solution:

$$S^* = \frac{(\gamma + \mu)N}{\beta}, \quad U^* = \frac{\mu}{\mu + \gamma}(N - S^*), \quad \text{and} \quad C^* = \frac{\gamma}{\mu} U^*. \quad (20)$$

Furthermore, let us define the basic reproduction number  $R_0$  (Chen et al. 2024) as

$$R_0 = \frac{\beta}{\mu + \gamma}. \quad (21)$$

The following tests are based on parameter values intentionally chosen from hypothetical scenarios to demonstrate the qualitative dynamics of the proposed model, rather than to reproduce or fit specific empirical data from real-world epidemics.

Figure 2(a) illustrates the evolution of  $S(t)$ ,  $U(t)$ , and  $C(t)$  for  $\alpha = 1$ . Here,  $\beta = 0.7$ ,  $\gamma = 1/4$ ,  $S_0 = 9470$ ,  $U_0 = 30$ ,  $C_0 = 500$ , and  $T = 90$  are used. From these parameter values, we have  $S^* = 4286$ ,  $U^* = 952$ ,  $C^* = 4762$ , and  $R_0 = 2.33$ .

The susceptible population,  $S(t)$ , begins at a high value, initially decreases sharply, undergoes oscillations, and eventually stabilizes at a steady level. The unidentified infected group,  $U(t)$ , exhibits an early peak with a rapid increase, followed by an oscillatory decline as more individuals are likely identified over time. The confirmed infected group,  $C(t)$ , increases more gradually, experiences oscillatory decreases, and ultimately levels off after reaching its peak. Figure 2(b) compares the temporal evolution of  $S(t)$  for different values of  $\alpha$  (1, 0.8, and 0.1). The susceptible population decreases faster when  $\alpha = 0.1$ , compared to the other values. As  $\alpha$  increases to 0.8 and 1, the behavior of  $S(t)$  shows a gradual decline in its minimum values over time, as seen in the figure. The plot

for  $\alpha = 0.1$  (red dashed line) drops quickly and monotonically, in contrast to  $\alpha = 0.8$  (black dotted line) and  $\alpha = 1$  (blue solid line), which show oscillatory behavior. Both  $\alpha = 0.8$  and  $\alpha = 1$  show similar trends in decline, but  $\alpha = 1$  exhibits a slower and more extended decrease before stabilizing. The results suggest that smaller  $\alpha$  values result in a more rapid initial decrease in the susceptible population. The analysis indicates that smaller  $\alpha$  values lead to a faster initial decrease in the susceptible population, while larger  $\alpha$  values result in a slower, oscillatory decline with lower minimum values before stabilization. Figure 2(c) shows the temporal evolution of  $U(t)$  for different values of  $\alpha$ . The unidentified infected population,  $U(t)$ , shows an initial increase in all cases but differs in magnitude and rate depending on  $\alpha$ . For  $\alpha = 1$ , the peak of  $U(t)$  is higher and occurs later, while lower  $\alpha$  values (0.8 and 0.1) show smaller peaks and faster growth. This indicates that the spread of infection varies with changes in  $\alpha$ . Figure 2(d) displays the temporal evolution of  $C(t)$  for different values of  $\alpha$ . The confirmed infected population,  $C(t)$ , increases steadily for all values of  $\alpha$ , but the rate of increase is initially faster when  $\alpha = 0.1$ . When  $\alpha = 1$ , the confirmed cases increase more gradually, reach a peak, and then decrease to a steady state.

The computational results indicate that smaller  $\alpha$  values lead to a faster initial decline in the susceptible population ( $S(t)$ ) and a quicker rise in the unidentified infected ( $U(t)$ ) and confirmed infected populations ( $C(t)$ ), while larger  $\alpha$  values, such as 1, result in slower, more oscillatory behavior across all groups. In particular, for  $\alpha = 1$ , the peaks in  $U(t)$  and  $C(t)$  are higher and occur later, with a gradual approach to steady states, while smaller  $\alpha$  values result in smaller peaks and faster monotonic growth. This shows that the dynamics of infection spread are strongly influenced by the value of  $\alpha$ .

Figure 3(a) displays the evolution of  $S(t)$ ,  $U(t)$ , and  $C(t)$  for  $\alpha = 1$ . Here,  $\beta = 0.7$ ,  $\gamma = 1/3$ ,  $S_0 = 9470$ ,  $U_0 = 30$ ,  $C_0 = 500$ , and  $T = 90$  are used. From these parameter values, we have  $S^* = 5476$ ,  $U^* = 590$ ,  $C^* = 3934$ , and  $R_0 = 1.83$ . The susceptible population starts high and decreases sharply, followed by oscillations and eventual stabilization. However, the stabilization point occurs at a slightly higher value than in Figure 2(a), likely due to the change in  $\gamma$ . The unidentified infected population  $U(t)$  reaches an early peak and then declines with oscillations, similar to Figure 2(a). The magnitude of the peak appears slightly lower. The confirmed infected population  $C(t)$  rises more gradually and eventually stabilizes

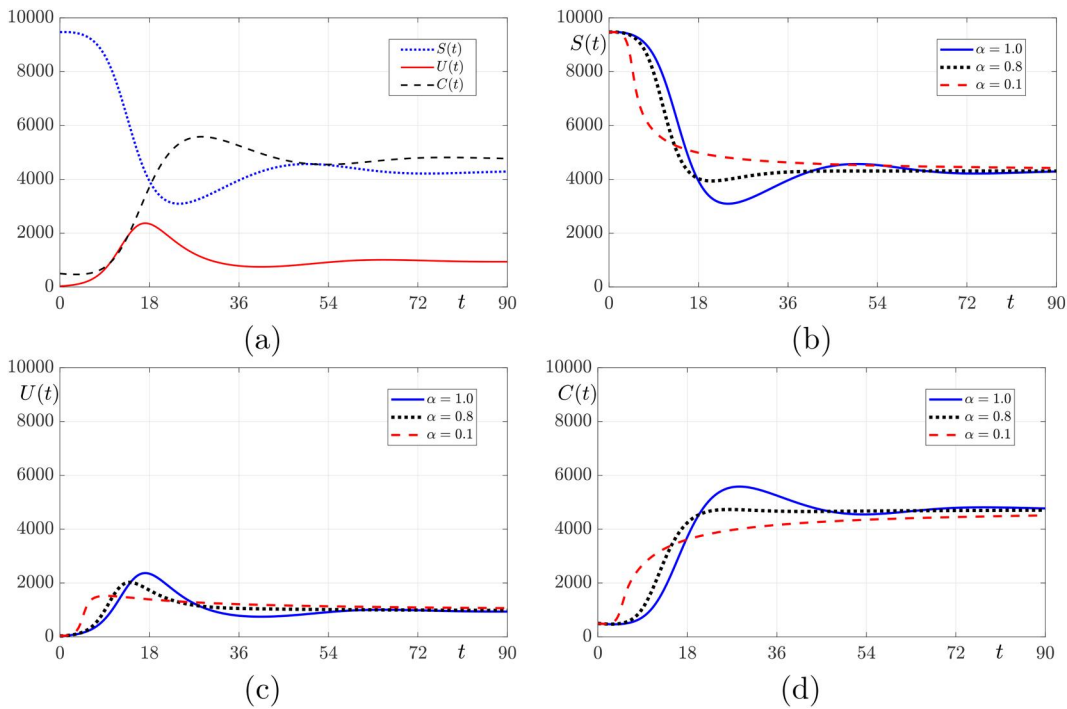


**Figure 2.** (a) Is the evolution of  $S(t)$ ,  $U(t)$ , and  $C(t)$  with  $\alpha = 1$ . (b), (c), and (d) are the evolutions of  $S(t)$ ,  $U(t)$ , and  $C(t)$ , respectively, with  $\alpha = 1, 0.8$ , and  $0.1$ . Here,  $\beta = 0.7$ ,  $\gamma = 1/4$ ,  $S_0 = 9470$ ,  $U_0 = 30$ ,  $C_0 = 500$ , and  $T = 90$  are used.

after reaching a peak. Compared to Figure 2(a), the increase is slower, and the final steady state is reached at a lower value, which indicates that the confirmed population stabilizes at a lower level in this scenario. Figure 3(b) shows a comparison of  $S(t)$  for different values of  $\alpha$  (1, 0.8, 0.1). Smaller  $\alpha$  values (like 0.1) lead to a faster decline in  $S(t)$ , while larger values of  $\alpha$  (1) result in a slower decline with more pronounced oscillations. However, in this case, the minimum values reached by  $S(t)$  are higher than in the previous case, which reflects the effect of changing  $\gamma$ . Figure 3(c) displays a comparison of  $U(t)$  for different values of  $\alpha$  (1, 0.8, 0.1). The unidentified infected population  $U(t)$  with smaller  $\alpha$  values results in earlier and smaller peaks, while larger  $\alpha$  values delay the peak and increase its magnitude. However, the peaks in Figure 3(c) are slightly lower and occur later than those in Figure 2(c). Figure 3(d) shows a comparison of  $C(t)$  for different values of  $\alpha$  (1, 0.8, 0.1). The confirmed infected population  $C(t)$  grows steadily, but the rate of growth and the timing of the peak vary with  $\alpha$ , as seen in Figure 2(d). In this case, the peak for  $\alpha = 1$  is lower than in Figure 2(d). The confirmed cases stabilize at a lower level. The key differences between Figures 2 and 3 are as follows: In Figure 3, with  $\gamma = 1/3$ , the overall infection dynamics are slower, and the susceptible population tends to stabilize at higher values compared to Figure 2 ( $\gamma = 1/4$ ). The peaks in both the unidentified and confirmed

infected populations are delayed, which indicates a longer period of infection spread. The peaks in  $U(t)$  and  $C(t)$  are generally lower in Figure 3, which suggests a less significant infection burden under the larger  $\gamma$  value.

## 5. Conclusions

The proposed normalized time-fractional SUC mathematical equation presented epidemiological dynamics by effectively integrating memory effects through fractional calculus. This model resolved the limitations of traditional integer-order models by capturing the persistent influence of past epidemic stages on current disease transmission and provided a more accurate representation of real-world infection patterns. Our simulation results demonstrated the critical role of the fractional order parameter  $\alpha$  and the confirmation parameter  $\gamma$  in computing the epidemic's progression. From the computational experiments, smaller  $\alpha$  values lead to a faster initial decline in the susceptible population and a quicker rise in unidentified and confirmed infected cases. Larger  $\alpha$  values result in slower, more oscillatory dynamics. This highlights the sensitivity of the infection model to the fractional order of the time derivatives. The change in  $\gamma$  from  $1/4$  (Figure 2) to  $1/3$  (Figure 3) results in slower dynamics overall, with more extended oscillations and a higher steady-state value of the susceptible

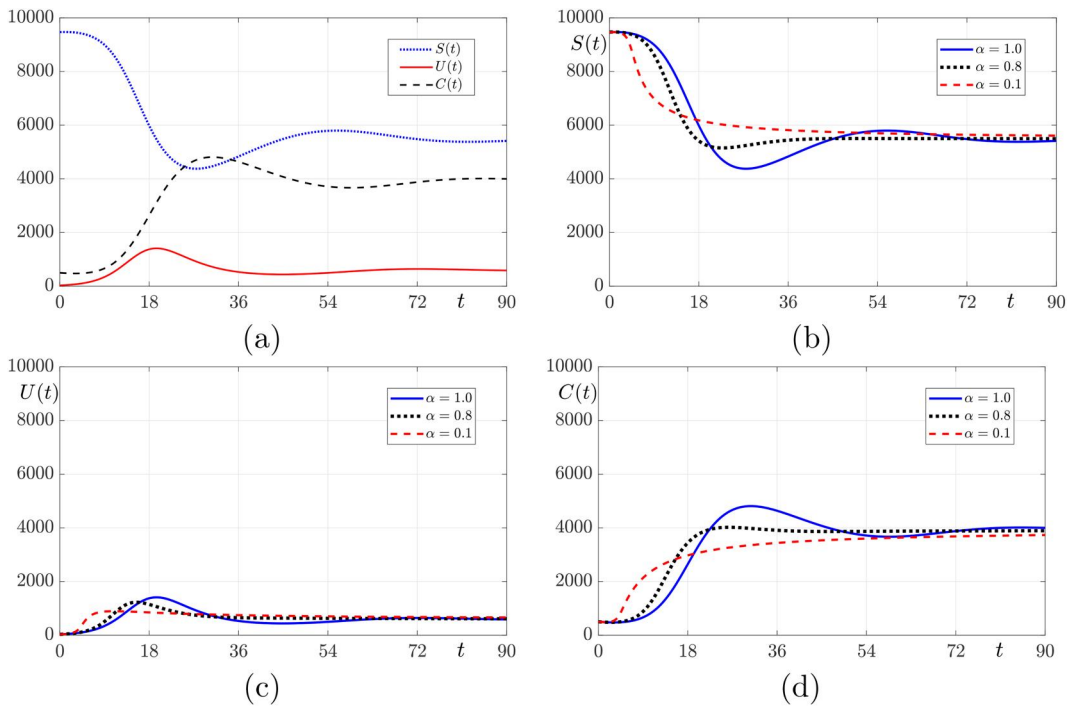


**Figure 3.** (a) Is the evolution of  $S(t)$ ,  $U(t)$ , and  $C(t)$  with  $\alpha = 1$ . (b), (c), and (d) are the evolutions of  $S(t)$ ,  $U(t)$ , and  $C(t)$ , respectively, with  $\alpha = 1, 0.8$ , and  $0.1$ . Here,  $\beta = 0.7$ ,  $\gamma = 1/3$ ,  $S_0 = 9470$ ,  $U_0 = 30$ ,  $C_0 = 500$ , and  $T = 90$  are used.

population. These findings show that the model can help understand and predict infectious disease progression and provide useful insights for public health and control strategies. Future work should include validation with real epidemiological data, the incorporation of demographic changes and additional compartments such as recovered and vaccinated groups, and a thorough sensitivity analysis of the fractional order parameter. Furthermore, an extension of the model to a spatially heterogeneous setting would improve its practical applicability.

## Authors contributions

**CRedit:** **Chaeyoung Lee:** Conceptualization, Formal analysis, Funding acquisition, Methodology, Resources, Validation, Writing – original draft, Writing – review & editing; **Soobin Kwak:** Conceptualization, Investigation, Validation, Writing – original draft, Writing – review & editing; **Yunjae Nam:** Data curation, Investigation, Visualization, Writing – original draft, Writing – review & editing; **Hyundong Kim:** Investigation, Methodology, Validation, Writing – original draft, Writing – review & editing; **Junseok Kim:** Conceptualization, Formal analysis, Methodology, Project administration, Software, Supervision, Validation, Visualization, Writing – original draft, Writing – review & editing.

## Acknowledgments

The authors express their gratitude to the reviewers for dedicating their time and effort to review the manuscript and for providing valuable feedback. Chaeyoung Lee: Conceptualization, Methodology, Validation, Formal analysis, Resources, Writing – Original Draft, Writing – Review and Editing; Jyoti: Validation, Formal analysis, Investigation, Writing – Original Draft, Writing – Review and Editing; Soobin Kwak: Conceptualization, Validation, Investigation, Writing – Original Draft, Writing – Review and Editing; Yunjae Nam: Investigation, Data Curation, Writing – Original Draft, Writing – Review and Editing, Visualization; Hyundong Kim: Methodology, Validation, Investigation, Writing – Original Draft, Writing – Review and Editing; Junseok Kim: Conceptualization, Methodology, Software, Validation, Formal analysis, Writing – Original Draft, Writing – Review and Editing, Visualization, Supervision, Project administration;

## Disclosure statement

The authors declare that they have no known competing financial interests or personal relationships that could have appeared to influence the work reported in this paper.

## Funding

The first author (C. Lee) was supported by the National Research Foundation of Korea (NRF) grant funded by the Korea government (MSIT) (No. 2022R1C1C2003896). The

corresponding author (J.S. Kim) was supported by Korea University Grant K2504591.

## Data availability statement

The datasets analysed in the current study are available from the corresponding author upon request.

## References

- Alharthi NH, Jeelani MB. 2023. Analyzing a Seir-type mathematical model of sars-covid-19 using piecewise fractional order operators. *MATH.* 8(11):27009–27032. doi: [10.3934/math.20231382](https://doi.org/10.3934/math.20231382).
- Alsaadi A, Dayan F, Ahmed N, Baleanu D, Rafiq M, Raza A. 2023. Evolutionary computational method for tuberculosis model with fuzziness. *AIP Adv.* 13(8):085125. doi: [10.1063/5.0165348](https://doi.org/10.1063/5.0165348).
- Ayouni I, Maatoug J, Dhouib W, Zammit N, Fredj SB, Ghammam R, Ghannem H. 2021. Effective public health measures to mitigate the spread of covid-19: a systematic review. *BMC Public Health.* 21(1):1015. doi: [10.1186/s12889-021-11111-1](https://doi.org/10.1186/s12889-021-11111-1).
- Baba IA, Rihan FA. 2022. A fractional-order model with different strains of covid-19. *Phys A.* 603:127813. doi: [10.1016/j.physa.2022.127813](https://doi.org/10.1016/j.physa.2022.127813).
- Besalú M, Binotto G. 2023. Time-dependent non-homogeneous stochastic epidemic model of sir type. *MATH.* 8(10):23218–23246. doi: [10.3934/math.20231181](https://doi.org/10.3934/math.20231181).
- Bouissa A, Tahiri M, Tsouli N, Sidi Ammi MR. 2023. Global dynamics of a time-fractional spatio-temporal sir model with a generalized incidence rate. *J Appl Math Comput.* 69(6):4779–4804. doi: [10.1007/s12190-023-01932-1](https://doi.org/10.1007/s12190-023-01932-1).
- Çar U, Çelik E. 2022. Analysis of COVID-19 disease with sir model and Taylor matrix method. *AIMS Math.* 7: 11188–11200. doi: [10.3934/math.2022626](https://doi.org/10.3934/math.2022626).
- Chen M, Kwak S, Ham S, Hwang Y, Kim J. 2024. Global stability analysis of an extended SUC epidemic mathematical model. *Z Naturforsch A.* 79(11):1033–1040. doi: [10.1515/zna-2024-0152](https://doi.org/10.1515/zna-2024-0152).
- Fan G, Li N. 2023. Application and analysis of a model with environmental transmission in a periodic environment. *ERA.* 31(9):5815–5844. doi: [10.3934/era.2023296](https://doi.org/10.3934/era.2023296).
- Fatima B, Rahman MU, Althobaiti A, Althobaiti A, Arfan M. 2024. Analysis of age wise fractional order problems for the COVID-19 under non-singular kernel of Mittag-Leffler law. *Comput Methods Biomed Eng.* 27(10):1303–1321. doi: [10.1080/10255842.2023.2239976](https://doi.org/10.1080/10255842.2023.2239976).
- Hwang Y, Kwak S, Kim J, Jyoti. 2024. Optimal time-dependent SUC model for COVID-19 pandemic in India. *BMC Infect Dis.* 24(1):1031. doi: [10.1186/s12879-024-09961-2](https://doi.org/10.1186/s12879-024-09961-2).
- Jornet M, Nieto JJ. 2024. Power-series solution of the l-fractional logistic equation. *Appl Math Lett.* 154: 109085. doi: [10.1016/j.aml.2024.109085](https://doi.org/10.1016/j.aml.2024.109085).
- Kim J. 2024. Influence of fractional order on the behavior of a normalized time-fractional sir model. *Mathematics.* 12(19):3081. doi: [10.3390/math12193081](https://doi.org/10.3390/math12193081).
- Korber B, Fischer WM, Gnanakaran S, Yoon H, Theiler J, Abfalterer W, Hengartner N, Giorgi EE, Bhattacharya T, Foley B, et al. 2020. Tracking changes in SARS-CoV-2 spike: evidence that d614g increases infectivity of the COVID-19 virus. *Cell.* 182(4):812–827.e19. doi: [10.1016/j.cell.2020.06.043](https://doi.org/10.1016/j.cell.2020.06.043).
- Lee C, Nam Y, Bang M, Ham S, Kim J. 2024. Numerical investigation of the dynamics for a normalized time-fractional diffusion equation. *MATH.* 9(10):26671–26687. doi: [10.3934/math.20241297](https://doi.org/10.3934/math.20241297).
- Li E, Zhang Q. 2023. Global dynamics of an endemic disease model with vaccination: analysis of the asymptomatic and symptomatic groups in complex networks. *ERA.* 31(10):6481–6504. doi: [10.3934/era.2023328](https://doi.org/10.3934/era.2023328).
- Liu Y, Yan L-M, Wan L, Xiang T-X, Le A, Liu J-M, Peiris M, Poon LLM, Zhang W. 2020. Viral dynamics in mild and severe cases of covid-19. *Lancet Infect Dis.* 20(6): 656–657. doi: [10.1016/S1473-3099\(20\)30232-2](https://doi.org/10.1016/S1473-3099(20)30232-2).
- Lv Z, Zeng J, Ding Y, Liu X. 2022. Stability analysis of time-delayed Sair model for duration of vaccine in the context of temporary immunity for COVID-19 situation. *ERA.* 31(2):1004–1030. doi: [10.3934/era.2023050](https://doi.org/10.3934/era.2023050).
- Majee S, Adak S, Jana S, Mandal M, Kar TK. 2022. Complex dynamics of a fractional-order sir system in the context of Covid-19. *J Appl Math Comput.* 68(6):4051–4074. doi: [10.1007/s12190-021-01681-z](https://doi.org/10.1007/s12190-021-01681-z).
- Salman AM, Ahmed I, Mohd MH, Jamiluddin MS, Dheyab MA. 2021. Scenario analysis of COVID-19 transmission dynamics in Malaysia with the possibility of reinfection and limited medical resources scenarios. *Comput Biol Med.* 133: 104372. doi: [10.1016/j.combiomed.2021.104372](https://doi.org/10.1016/j.combiomed.2021.104372).
- Santra PK, Mahapatra GS, Basu S. 2024. Stability analysis of fractional epidemic model for two infected classes incorporating hospitalization impact. *Phys Scr.* 99(6):065237. doi: [10.1088/1402-4896/ad4692](https://doi.org/10.1088/1402-4896/ad4692).
- Sene N. 2020. Sir epidemic model with Mittag-Leffler fractional derivative. *Chaos Solitons Fractals.* 137:109833. doi: [10.1016/j.chaos.2020.109833](https://doi.org/10.1016/j.chaos.2020.109833).
- Shahabifar R, Molavi-Arabshahi M, Nikan O. 2024. Numerical analysis of covid-19 model with caputo fractional order derivative. *AIP Adv.* 14(3):035202. doi: [10.1063/5.0189939](https://doi.org/10.1063/5.0189939).
- Shaikh AS, Shaikh IN, Nisar KS. 2020. A mathematical model of covid-19 using fractional derivative: outbreak in India with dynamics of transmission and control. *Adv Differ Equ.* 2020(1):373. doi: [10.1186/s13662-020-02834-3](https://doi.org/10.1186/s13662-020-02834-3).
- Thirumalai S, Yüzbaşı Ş, Seshadri R. 2025. A numerical investigation of fractional measles epidemic model using Chebyshev spectral collocation method. *Comput Methods Biomed Eng.* 1–25. doi: [10.1080/10255842.2025.2485374](https://doi.org/10.1080/10255842.2025.2485374).
- Ur Rahman M, Boulaaras S, Tabassum S, Baleanu D. 2025. A deep neural network analysis of fractional omicron mathematical model with vaccination and booster dose. *Alex Eng J.* 118:435–448. doi: [10.1016/j.aej.2025.01.072](https://doi.org/10.1016/j.aej.2025.01.072).
- Williams BA, Jones CH, Welch V, True JM. 2023. Outlook of pandemic preparedness in a post-COVID-19 world. *NPJ Vaccines.* 8(1):178. doi: [10.1038/s41541-023-00773-0](https://doi.org/10.1038/s41541-023-00773-0).
- Witbooi PJ, Vyambwera SM, Nsuami MU. 2023. Control and elimination in an seir model for the disease dynamics of COVID-19 with vaccination. *MATH.* 8(4):8144–8161. doi: [10.3934/math.2023411](https://doi.org/10.3934/math.2023411).

- Xu Z, Liu K, Gao GF. 2022. Omicron variant of SARS-CoV-2 imposes a new challenge for the global public health. *Biosaf Health*. 4(3):147–149. doi: [10.1016/j.bsheal.2022.01.002](https://doi.org/10.1016/j.bsheal.2022.01.002).
- Yang J, Li Y, Kim J. 2024. Phase-field modeling and linearly energy-stable Runge–Kutta algorithm of colloidal crystals on curved surfaces. *J. Comput. Appl. Math.* 443:115750. doi: [10.1016/j.cam.2023.115750](https://doi.org/10.1016/j.cam.2023.115750).
- Yousif R, Jeribi A, Al-Azzawi S. 2023. Fractional-order Seird model for global covid-19 outbreak. *Mathematics*. 11(4):1036. doi: [10.3390/math11041036](https://doi.org/10.3390/math11041036).
- Zahrani SMAI, Elsmih FEI, Zahrani KSAl, Saber S. 2022. A fractional order SITR model for forecasting of transmission of COVID-19: sensitivity statistical analysis. *MJMS*. 16(3):517–536. doi: [10.47836/mjms.16.3.08](https://doi.org/10.47836/mjms.16.3.08).
- Zhang Y, Yu X, Sun H, Tick GR, Wei W, Jin B. 2020. Applicability of time fractional derivative models for simulating the dynamics and mitigation scenarios of covid-19. *Chaos Solitons Fractals*. 138:109959. doi: [10.1016/j.chaos.2020.109959](https://doi.org/10.1016/j.chaos.2020.109959).
- Zhao X, Shi J. 2023. Dynamic behavior of a stochastic sir model with nonlinear incidence and recovery rates. *MATH*. 8(10):25037–25059. doi: [10.3934/math.20231278](https://doi.org/10.3934/math.20231278).

## Appendix

The MATLAB code is provided as follows:

```

clear ; % Clear workspace
T=90; % Total simulation time
dt = 1.0 e -1; % Initial time step size
Nt = round (T / dt); % Number of time steps (rounded)
dt=T / Nt ; % Recompute dt so that Nt*dt=T exactly
b=0.7; % Infection/contact rate parameter
g=0.25; % Recovery rate parameter
mu = 0.05; % Natural removal rate parameter
N=10000; % Total population size
U (1) = 30; % Initial number of U individuals
C (1) = 500; % Initial number of C individuals
S (1) = N - U (1) - C (1); % Initial number of S individuals
R0=b / (g+mu); % Basic reproduction number
SS=N / R0; % Disease-free equilibrium for S
US=mu * N * (R0 - 1) / b; % Equilibrium for U
CS=N - SS - US; % Equilibrium for C
alphadata =[1 0.1 0.8]; % Array of fractional orders alpha to simulate

for k = 1: length (alphadata)
    if k == 1
        flag = 1; % Use standard Euler scheme for alpha = 1
    else
        flag = 2; % Use fractional update scheme for 0 < alpha < 1
    end
    beta = alphadata (k); % Current fractional order alpha

    for iter = 1: Nt
        % Compute fractional weights w(q) for memory term
        for q = 1: it
            w (q)=((it +1- q)^(1- beta)-(it - q)^(1- beta))/ it ^ (1- beta);
        end
        G1=0; G2=0; % Initialize convolution sums
        if it > 1 % Compute history integrals for S and U
            for q = 1: it -1
                G1=G1+w (q) * (S (q +1) - S (q)) / dt ;
                G2=G2+w (q) * (U (q +1) - U (q)) / dt ;
            end
        end
        if flag == 1
            % Classical Euler update (alpha = 1)
            S (it +1)=S (it)+ dt *(mu * N - b * S (it)* U (it)/ N - mu * S (it));
            U (it +1)= U (it)+ dt *(b * S (it)* U (it)/ N - g * U (it)- mu * U (it));
        else
            % Fractional update (0 < alpha < 1) using weight w(it)
            S (it +1)=(w (it)* S (it)/ dt + mu * N - G1)/(w (it)/ dt + b * U (it)/ N + mu);
            U (it +1)=(w (it)* U (it)/ dt + b * S (it +1)* U (it)/ N - G2)/(w (it)/ dt + g + mu);
        end
        end
        C=N - S - U ; % Compute C from conservation
        DS (:, k) = S ' ; % Store S time series for plotting
        DU(:,k) = U' ; % Store U time series
        DC(:,k) = C' ; % Store C time series
    end
end

```

```
% Plot results for alpha = 1
Figure (1); clf;
t=linspace(0, dt*Nt, Nt + 1); % Time vector
set(gcf, 'position', [200 500 600 300])
plot(t, DS(:,1), 'r-'); hold on; grid on
plot(t, DU(:,1), 'b-'); plot(t, DC(:,1), 'm-');
set(gca, 'fontsize', 17);
lgd=legend('S(t)''U(t)' 'C(t)', 'Interpreter', ...
' latex', ' fontsize', 13);
set(lgd, 'Position', [0.7, 0.7, 0.15, 0.15]); axis([0 T 0 N]);
xlabel('Time $ t $', 'Interpreter', ' latex', 'FontSize', 20);
% Plot comparison across fractional orders
for i=2:4
    figure(i); clf;
    set(gcf, 'position', [200 500 600 300])
    if i == 2 % Plot S(t) for alpha = 1.0, 0.8, 0.1
        plot(t, DS(:,1), 'b-'); hold on;
        plot(t, DS(:,3), 'k-'); plot(t, DS(:,2), 'r-');
    elseif i == 3 % Plot U(t) for alpha = 1.0, 0.8, 0.1
        plot(t, DU(:,1), 'b-'); hold on;
        plot(t, DU(:,3), 'k-'); plot(t, DU(:,2), 'r-');
    else % Plot C(t) for alpha = 1.0, 0.8, 0.1
        plot(t, DC(:,1), 'b-'); hold on;
        plot(t, DC(:,3), 'k-'); plot(t, DC(:,2), 'r-');
    end
    grid on; set(gca, 'fontsize', 17);
    lgd=legend('$\alpha = 1.0$', '$\alpha = 0.8$', '$\alpha = 0.1$', ...
'Interpreter', ' latex', ' fontsize', 13);
    set(lgd, 'Position', [0.7, 0.7, 0.15, 0.15]);
    xlabel('Time $ t $', 'Interpreter', ' latex', 'FontSize', 20);
    % Label the variable on the plot
    if i == 2
        ylabel('S(t)', 'Interpreter', ' latex', 'FontSize', 16);
    elseif i == 3
        ylabel('U(t)', 'Interpreter', ' latex', 'FontSize', 16);
    else
        ylabel('C(t)', 'Interpreter', ' latex', 'FontSize', 16);
    end
    axis([0 T 0 N])
end
```